Digital Signal Processing 78 (2018) 185–196

Contents lists available at ScienceDirect

Digital Signal Processing

www.elsevier.com/locate/dsp

Fourier–Bessel series expansion based empirical wavelet transform for analysis of non-stationary signals

Abhijit Bhattacharyya *, Lokesh Singh, Ram Bilas Pachori

Discipline of Electrical Engineering, Indian Institute of Technology Indore, Indore-453552, India

ARTICLE INFO

Article history:
Available online 7 March 2018

Keywords:
Empirical wavelet transform (EWT)
Fourier–Bessel series expansion (FBSE)
Normalized Hilbert transform (NHT)
Time–frequency (TF) representation

ABSTRACT

In this paper, a new method has been presented for the time–frequency (TF) representation of non-stationary signals. The existing empirical wavelet transform (EWT) has been enhanced using Fourier–Bessel series expansion (FBSE) in order to obtain improved TF representation of non-stationary signals. We have used the FBSE method for the spectral representation of the analyzed multi-component signals with good frequency resolution. The scale-space based boundary detection method has been applied for the accurate estimation of boundary frequencies in the FBSE based spectrum of the signal. After that, wavelet based filter banks have been generated in order to decompose non-stationary multi-component signals into narrow-band components. Finally, the normalized Hilbert transform has been applied for the estimation of amplitude envelope and instantaneous frequency functions from the narrow-band components and obtained the TF representation of the analyzed non-stationary signal. We have applied our proposed method for the TF representation of multi-component synthetic signals and real electroencephalogram (EEG) signals. The proposed method has provided better TF representation as compared to existing EWT method and Hilbert–Huang transform (HHT) method, especially when analyzed signal possesses closed frequency components and of short time duration.

1. Introduction

Non-stationary signal analysis methods are focused to model the inherent time-varying characteristics of the analyzed signals recorded in several areas namely, communications, speech analysis and synthesis, radar, biomedical, and mechanical engineering [1]. The conventional Fourier transform (FT) based methods are not well suited for the spectral analysis of such signals. Moreover, the real life complicated biological signals [2–5], finance signals [6], civil structure vibration signals [7,8] are highly non-stationary in nature which require adequate analysis based on their information content.

In literature, several time–frequency (TF) domain based methods exist for analysing non-stationary signals namely short-time FT (STFT) [9], wavelet transform (WT) [10], Wigner–Ville distribution (WVD) [1], and Hilbert–Huang transform (HHT) [11]. The features can be extracted in TF domain for the classification of non-stationary signals [12]. The STFT provides TF representation of non-stationary signals based on moving window concept. But, the use of fixed moving window imposes a trade off between time and frequency resolutions in TF plane [13]. In order to overcome the limitations of STFT, the WT was proposed for the efficient TF representation of non-stationary signals. The WT uses pre-fixed basis functions and decomposes signals into different oscillatory levels with the transient characteristics of the analyzed signals retained [14]. However, due to predefined filter banks, WT fails to decompose signals according to the presence of information content. Therefore, it is difficult to determine instantaneous amplitude (IA) and instantaneous frequency (IF) functions from the decomposed components corresponding to actual mono-component signals. The wavelet packet transform [15,16] was proposed in order to enhance signal adaptability. However, this approach is still limited by the use of prefixed basis functions. In [17], authors proposed tunable-Q wavelet transform (TQWT) for the analysis of non-stationary signals. In TQWT method, the Q factor of the wavelet transform can be tuned in accordance to the oscillatory nature of the signal. In [18], authors proposed synchrosqueezed wavelet transform as the combination of wavelet transform and reallocation methods. This method achieved better TF resolution as compared to conventional wavelet transform. In [19], authors introduced variational mode decomposition (VMD) method which decomposes real valued signal into finite number of components. The VMD method has been found suitable for analysing non-stationary signals and applied in [20] for instantaneous voiced and

* Corresponding author.
E-mail addresses: phd1401202001@iiti.ac.in (A. Bhattacharyya), mt1602102005@iiti.ac.in (L. Singh), pachori@iiti.ac.in (R.B. Pachori).

https://doi.org/10.1016/j.dsp.2018.02.020
1051-2004/

non-voiced detection from speech signals and in [21] for speech enhancement.

Majority of the existing methods rely on pre-fixed basis functions to analyze the signals and hence are considered to be rigid or non-adaptive. However, the non-adaptive methods find difficulty in analyzing physical signals due to the existence of closely spaced frequency components. In the HHT [11] based TF representation, empirical mode decomposition (EMD) method adaptively decomposes analyzed signals into amplitude and frequency modulated (AFM) components known as intrinsic mode functions (IMFs). Later, the Hilbert transform (HT) was applied in each of the IMFs for the estimation of IA and IF functions and TF representation was generated. In [22], authors proposed empirical decomposition method for separating amplitude modulation (AM) and frequency modulation (FM) parts from each IMF in order to estimate more meaningful IFs. In [23], authors cancelled the occurrences of riding waves from the empirically decomposed FM parts of the IMFs. However, the EMD method suffers from mode mixing problem and thus, IF functions cannot be effectively estimated [24]. In [25], authors proposed adaptive Fourier decomposition method in order to decompose non-stationary signals into a number of Fourier intrinsic band functions and provided time–frequency–energy distribution of the analyzed signals. In [26], authors introduced swarm decomposition based on fosters rules of biological swarms for the analysis of non-stationary signals. The method achieved good performance in extracting the components from the analyzed signals. In [27], TF representation was proposed using improved eigenvalue decomposition of the Hankel matrix together with HT. The TF representation using WVD is highly affected by the presence of cross-terms between the signal components [28,29]. This puts a major limitation towards the efficient estimation of instantaneous frequencies of the analyzed signals in multi-component situation.

In [30], empirical wavelet transform (EWT) was proposed for the analysis of non-stationary signals. In [31], the authors explored EWT method for multivariate signals and EWT based multivariate TF representation was proposed. It should be noted that, EWT is an adaptive decomposition method which extracts narrow-band frequency components from the analyzed signal based on the frequency information content in the signal spectrum. It decomposes signals with adaptive wavelet based filters after finding the boundary frequencies in the FT based spectrum. The computation of FT has been performed using fast FT (FFT) algorithm. The TF representation based on EWT, can be obtained after applying the HT on the narrow-band frequency components. However, EWT fails to represent closely spaced frequency components in the TF plane [32]. Moreover, it is very difficult to estimate the accurate frequency components for the short duration signals using EWT method due to the use of Fourier spectrum.

Thus, an improved method is desirable in order to encounter the aforementioned shortcomings of the existing EWT method. In this work, the conventional FT based spectrum has been replaced with the spectrum obtained using Fourier–Bessel series expansion (FBSE). It should be noted that, FBSE coefficients are useful for the spectral analysis of non-stationary signals due to the non-stationary nature of Bessel functions bases in the FBSE [33–35]. We have employed the existing scale-space based boundary detection method for the spectrum segmentation purpose. Finally, the normalized Hilbert transform (NHT) [22] based TF representation has been generated for analysing multi-component non-stationary signals. The proposed method has been applied on synthetically generated multi-component AM and FM signals as well as on real electroencephalogram (EEG) signals. We have obtained better TF representation using proposed FBSE-EWT method as compared to existing EWT and HHT based TF representations for the considered cases.

Table 1
Mathematical expressions of EWT scaling and wavelet functions.

Functions	Mathematical representation
Scaling [30]	$\Lambda_i(\omega) = \begin{cases} 1, & \text{if } \lvert\omega\rvert \le (1-\xi)\omega_i. \\ \cos\left(\frac{\pi\eta(\xi,\omega_i)}{2}\right), & \text{if } (1-\xi)\omega_i \le \lvert\omega\rvert \le (1+\xi)\omega_i. \\ 0, & \text{otherwise} \end{cases}$
Wavelet [30]	$\Theta_i(\omega) = \begin{cases} 1, & \\ & \text{if } (1+\xi)\omega_i \le \lvert\omega\rvert \le (1-\xi)\omega_{i+1}. \\ \cos\left(\frac{\pi\eta(\xi,\omega_{i+1})}{2}\right), & \\ & \text{if } (1-\xi)\omega_{i+1} \le \lvert\omega\rvert \le (1+\xi)\omega_{i+1}. \\ \sin\left(\frac{\pi\eta(\xi,\omega_i)}{2}\right), & \\ & \text{if } (1-\xi)\omega_i \le \lvert\omega\rvert \le (1+\xi)\omega_i. \\ 0, \text{ otherwise.} & \end{cases}$

The reminder of the paper is organised as follows: Section 2 briefly discusses the existing methods, Section 3 demonstrates the proposed method. The experimental results have been presented in Section 4, while Section 5 discusses the effectiveness of the proposed method. Finally, Section 6 concludes the paper.

2. A brief explanation of EWT, boundary detection based on scale-space representation, FBSE, normalized Hilbert transform, and performance evaluation measure

Here, in the following sub-sections, we have described the EWT method, the scale-space representation, the FBSE based spectrum representation, the NHT based TF representation, and performance evaluation in terms of mean square error (MSE) measure.

2.1. Empirical wavelet transform

The EWT is an adaptive signal decomposition method which was proposed in [30] for the analysis of non-stationary signals. The inherent mechanism of EWT is based on the formation of adaptive wavelet based filters. These wavelet based filters possess support in the spectrum information location of the analyzed signal. The obtained sub-band signals after EWT decomposition have specific center frequencies with compact frequency supports. The EWT method is summarised in the following steps [30]:

1. The FT method is used to obtain frequency spectrum of the analyzed signal in the frequency range $[0, \pi]$.
2. The frequency spectrum is segmented into N number of contiguous segments using EWT boundary detection method. In this work, we have used scale-space based boundary detection method [36] in order to find optimal set of boundary frequencies denoted as ω_i. In the next subsection, the scale-space based boundary detection method is discussed in brief. It should be noted that, the first and last boundary frequencies are prefixed to 0 and π, respectively. Thus, EWT boundary detection method is used to find the rest of the $N-1$ intermediate boundary frequencies.
3. The empirical scaling and wavelet functions are defined in each segment as the set of band-pass filters. The idea of construction of Littlewood–Paley and Meyer's wavelets is used for the construction of wavelet based filters [10,30].

The mathematical expressions of empirical scaling function $\Lambda_i(\omega)$ and wavelet function $\Theta_i(\omega)$ have been presented in Table 1. In the table, the function $\eta(\xi, \omega_i)$ is expressed as [30],

$$\eta(\xi, \omega_i) = \psi\left(\frac{(|\omega| - (1-\xi)\omega_i)}{2\xi\omega_i}\right) \tag{1}$$

where $\psi(z)$ is an arbitrary function defined as [30],

$$\psi(z) = \begin{cases} 0, & \text{if } z \leq 0. \\ \text{and } \psi(z) + \psi(1-z) = 1, & \forall z \in [0\ \ 1] \\ 1, & \text{if } z \geq 1. \end{cases} \tag{2}$$

The parameter ξ in Table 1 makes sure that empirical wavelets and scaling function form a tight frame in $L_2(R)$. The tight frame condition is expressed as follows [30]:

$$\xi < \min_i \left(\frac{\omega_{i+1} - \omega_i}{\omega_{i+1} + \omega_i} \right) \tag{3}$$

Now, the detail and approximation coefficients can be determined by taking the inner product of the analyzed signal with wavelets and scaling function which are expressed as [30],

$$\mathbf{V}_{y,\Theta}(i,t) = \int y(\tau)\overline{\Theta_i(\tau - t)}d\tau \tag{4}$$

$$\mathbf{V}_{y,\Lambda}(0,t) = \int y(\tau)\overline{\Lambda_1(\tau - t)}d\tau \tag{5}$$

where $\mathbf{V}_{y,\Theta}(i,t)$ denotes the detail coefficients of ith oscillatory level, whereas $\mathbf{V}_{y,\Lambda}(0,t)$ denotes the approximation coefficients.

Finally, the reconstructed sub-band signals can be defined as [30],

$$f_0(t) = \mathbf{V}_{y,\Lambda}(0,t) \star \Lambda_1(t) \tag{6}$$

$$f_i(t) = \mathbf{V}_{y,\Theta}(i,t) \star \Theta_i(t) \tag{7}$$

where $f_0(t)$ is the approximation sub-band signal and $f_i(t)$ denotes detail sub-band signal of ith level. The asterisk symbol denotes convolution operation in eqns (6) and (7).

2.2. Boundary detection based on scale-space representation

The scale-space representation of a discrete signal $x(n)$ can be obtained by computing the convolution of the signal with the Gaussian kernel, which is expressed as [36],

$$\Upsilon(m,t) = \sum_{n=-M}^{M} x(m-n) f(n;t) \tag{8}$$

where,

$$f(n;t) = \frac{1}{\sqrt{2\pi t}} \mathrm{e}^{\frac{-n^2}{2t}} \tag{9}$$

where $M = D\sqrt{t} + 1$ with $3 \leq D \leq 6$ and t is known as scale parameter. It should be noted that, as the scale parameter or scale-step parameter ($\rho = \sqrt{\frac{t}{t_o}}$, $\rho = 1, 2, \ldots \rho_{\max}$) increases, the number of minima decreases in the scale-space plane and no new minima appears. Let the total number of initial minima is denoted by N_0. Thus, each of the initial minima P_i leads to a curve D_i in the scale-space plane of length R_i, where i varies from 1 to N_0. The length (integer) R_i is considered as life time of minima i (not equal to the arc length of D_i) and expressed as $R_i = \max\{\rho/\text{the } i\text{th minimum exists}\}$. Using this concept, the meaningful modes are defined in the histogram, as follows: The support of a meaningful mode should be delimited by two local minima which lead to two long (greater than a threshold T_h) scale-space curves D_i. Therefore, the optimal threshold (T_h) should be determined in order to select the scale-space curves of length higher than threshold value. Finally, the Ostu's method [37,36] has been used for determining the threshold value T_h and meaningful modes have been found.

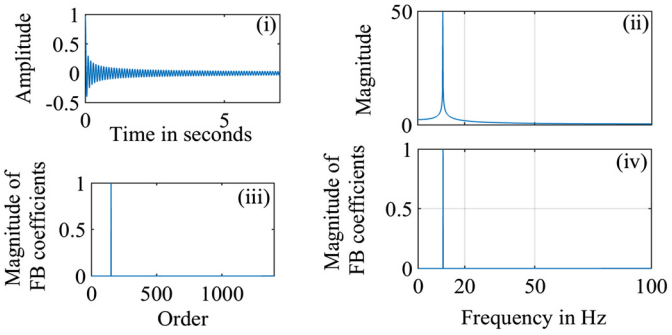

Fig. 1. (i) Plot of an arbitrary Bessel basis function (ii) Plot of FT of the considered Bessel basis function (iii) Plot of FB coefficients of the considered Bessel basis function, (iv) Plot of the FBSE spectrum.

2.3. Fourier–Bessel series expansion

The FBSE uses Bessel functions as bases, which are non-stationary in nature. This makes FBSE suitable for analysis of signals with time-varying parameters.

The FBSE of $y(n)$ using zero-order Bessel functions is expressed as follows [38–40]:

$$y(n) = \sum_{i=1}^{U} C_i J_0\left(\frac{\beta_i n}{U}\right),\ n = 0, 1, \ldots, U-1 \tag{10}$$

where, C_i are known as the Fourier–Bessel (FB) series coefficients of $y(n)$ which can be expressed as follows [38,39]:

$$C_i = \frac{2}{U^2 (J_1(\beta_i))^2} \sum_{n=0}^{U-1} n y(n) J_0\left(\frac{\beta_i n}{U}\right) \tag{11}$$

where, $J_0(.)$ and $J_1(.)$ denote zero and first-order Bessel functions, respectively. The positive roots (in the ascending order) of the zero-order Bessel function ($J_0(\beta) = 0$) are denoted by β_i with $i = 1, 2, \cdots U$. It should be noted that, order i of the FB series coefficients is related to continuous-time frequency f_i (in Hz) where it has the peak value, by the following equation [38,39]:

$$\beta_i \approx \frac{2\pi f_i U}{f_s},\ \text{where } \beta_i \approx \beta_{i-1} + \pi \approx i\pi \tag{12}$$

In equation (12), f_s denotes the sampling frequency.

The equation (12) can be expressed as [39,41],

$$i \approx \frac{2 f_i U}{f_s} \tag{13}$$

Hence, it is clear from equation (13) that, i should be varied from 1 to U (discrete-time signal length) in order to cover the entire bandwidth of the analyzed discrete-time signal. Thus, FBSE spectrum is the plot of magnitude of the FB coefficients ($|C_i|$) versus frequencies (f_i).

The spectral representation using FBSE has some advantages over conventional FT based spectral representation as follows:

Firstly, FBSE spectrum has compact representation as compared to conventional Fourier representation [42,34]. Fig. 1(i) presents the plot of an arbitrary Bessel basis function ($J_0(\frac{\beta_{150} n}{U}), U = 1400$) with 200 Hz sampling frequency. Fig. 1(ii) shows its Fourier spectrum. It can be seen in the figure that Bessel function has time-varying amplitude (decays with time). In [43] authors found that effective bandwidth of a signal is the contribution from AM bandwidth and FM bandwidth. Thus, a significant part of the total bandwidth of a Bessel function arises due to its AM nature. As a result, they have specific center frequency with finite bandwidth in the FT spectrum. This is in contrast to sinusoidal basis functions

of the FT, which do not contain AM and represented by spectral lines only. Fig. 1(iii) and (iv) show the plots of FBSE coefficients versus their orders and frequencies, respectively. It is clearly visible that the same finite bandwidth signal is represented by a single coefficient in FBSE domain. On the other side, it is obvious that a sinusoidal wave which is a basis function in FT, will be more compactly represented in the FT domain as compared to FBSE domain due to similarity of basis function with the analyzed signal. In that scenario, more FB coefficients are necessary for the representation of sinusoidal signals. However, real life signals like speech can be represented in terms of AFM components [44,45]. Such modelling approach is useful to represent wide-band signal in terms of narrow-band signals (AFM components). As shown in Fig. 1, the basis function which is used in FBSE has narrow-band nature in FT domain and represented compactly in FBSE domain. Such property helps to obtain more compact representation in FBSE domain as compared to FT domain for wide-band and non-stationary signals. This is because of the contribution of band of frequencies in the representation using Bessel basis functions in the FBSE. On the other hand, in FT based spectrum, sinusoidal basis functions represent spectral lines which do not have any finite bandwidth in frequency domain. Due to this reason, FT based spectrum is expected to have less compact representation as compared to FBSE spectrum. Hence, it is more likely that a band-pass signal will have more compact representation with fewer non-zero real FB coefficients in the FBSE spectrum.

Secondly, FBSE spectrum avoids the effect of windowing for spectral representation [39]. The FT based spectral representation is embedded with window function in order to reduce the effect of spectral leakage. However, the multiplication of the window function with signal produces AM and end points distortion in the time-domain. On the other hand, FBSE spectrum can produce signal characteristics even for short duration signals without the effect of windowing.

Moreover, spectral representation using FBSE requires the number of coefficients equal to the length of the discrete signal. This is contrary to the conventional FT spectrum where the spectrum length is half of the analyzed discrete signal [34]. Thus, FBSE based spectrum provides better spectral resolution as compared to FT spectrum. The zero-padding with signal for obtaining same length FT spectrum will produce only interpolated spectrum with smoother appearance. In practice, the resolution of the transform does not improve since number of points which provides the actual information remains same [46]. The extra points appearing in the FT spectrum after zero-padding will not provide any extra spectral information of the signal. They will be simply interpolated values. In case of FBSE spectrum, all the FB coefficients are unique for the analyzed signal [47,48].

These features of the FBSE spectrum help us to determine the optimal boundary frequencies more accurately as compared to FT spectrum, especially when the signal is of short length and contains closed frequency components.

2.4. Normalized Hilbert transform

The HT is used to compute IA and IF functions from the narrow-band signal components. The analytic signal representation using HT of narrow-band AFM signal $y(t)$ is expressed as [11],

$$y_h(t) = y(t) + jH[y(t)] \tag{14}$$

where, H is the HT operator.

In another way, eqn (14) is represented as,

$$y_h(t) = A(t)e^{j\phi(t)} \tag{15}$$

The IA function $A(t)$ and instantaneous phase $\phi(t)$ are represented as,

$$A(t) = \sqrt{y^2(t) + (H[y(t)])^2} \tag{16}$$

$$\phi(t) = \arctan\left(\frac{H[y(t)]}{y(t)}\right) \tag{17}$$

The IF function $f(t)$ is represented as,

$$f(t) = \frac{1}{2\pi}\frac{d}{dt}[\phi(t)] \tag{18}$$

However, Nuttall and Bedrosian in [49], imposed an important condition for getting a meaningful analytic signal for IF computation. This imposes a limitation of separating the HT of the carrier signal from its own envelope and can be expressed as,

$$H\{\alpha(t)\cos(\theta(t))\} = \alpha(t)H\{\cos(\theta(t))\} \tag{19}$$

provided that FT of the carrier signal and its envelope do not overlap. Thus the signal has to be mono-component and narrow-band as well. Otherwise, the FM part will be contaminated with AM variations. Thus, eqns (14) to (18) become no longer valid when the analyzed signal violates the condition mentioned in eqn (19).

In [22], the authors proposed NHT in order to get rid of Bedrosian condition [49]. They empirically decomposed AFM signals into envelope (AM) and carrier (FM) waves. The empirical AFM decomposition is summarised below [22].

It requires identification of all the local maxima points from the absolute value of given AFM signal $y(t)$ and connect them with a cubic spline. This spline curve $e_1(t)$ is termed as the envelope of the signal. Now, this obtained envelope is used to normalize the signal $y(t)$. The normalized signal $s_1(t)$ can be expressed as,

$$s_1(t) = \frac{y(t)}{e_1(t)} \tag{20}$$

After normalization, the signal $s_1(t)$ should satisfy the condition $|s_1(t)| \leq 1$. Otherwise, the envelope $e_2(t)$ of the signal $s_1(t)$ is found and the normalization process is again repeated, which is expressed as,

$$s_2(t) = \frac{s_1(t)}{e_2(t)} \tag{21}$$

After nth iteration, the signal $s_n(t)$ satisfies the condition $|s_n(t)| \leq 1$ and the normalization process is complete. Then, $s_n(t)$ is designated as empirically found FM part $F(t)$ of the AFM signal $y(t)$. It can be expressed as follows:

$$F(t) = s_n(t) = \cos(\phi(t)) \tag{22}$$

Then, the AM part $A(t)$ of the AFM signal is determined as,

$$A(t) = e_1(t)e_2(t)\ldots e_n(t) \tag{23}$$

Finally, the AFM signal $y(t)$ is expressed as,

$$y(t) = A(t)F(t) = A(t)\cos(\phi(t)) \tag{24}$$

Now, as the empirically obtained FM signal $F(t)$ satisfies $|F(t)| \leq 1$, the condition mentioned in eqn (19) is not violated and the computation of analytic signal through HT of $F(t)$ is no longer a concern [22]. Thus, IF, $f(t)$ is computed from the FM signal $F(t)$ using analytic signal representation by following eqns (14) to (18). In Fig. 2, we have shown the plots of an arbitrary AFM signal and its IAs and IFs using both HT and NHT methods. It can be observed that NHT provides better IF estimation of the considered AFM signal. Thus, we have used NHT for computation of the IA and IF throughout this work.

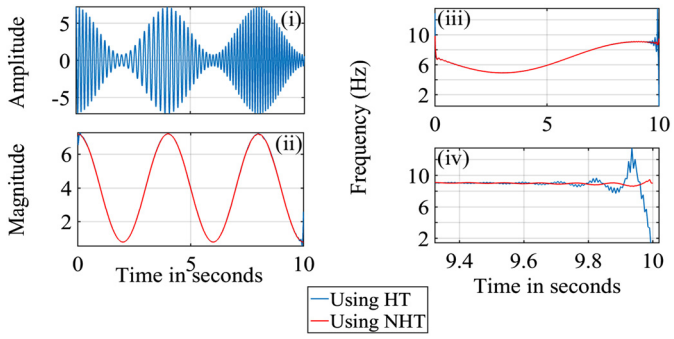

Fig. 2. (i) Plot of an arbitrary AFM signal $y(t) = 4(1 + 0.8\cos(0.5\pi t))\cos(2\pi(7t + 4\cos(0.52t)))$ with 200 Hz sampling frequency. Plot of (ii) IA and (iii) IF of the signal using HT and NHT methods, (iv) Plot of the zoomed version of the computed IF.

Finally, the TF coefficients considering all the N oscillatory levels, are expressed as follows [31]:

$$\mathrm{Tf}(f,t) = \sum_{i=1}^{N} A_i(t)\delta[f - f_i(t)] \tag{25}$$

where $A_i(t)$ and $f_i(t)$ denote IA and IF functions of ith oscillatory level.

3. Proposed method

In the proposed method, we have used FBSE in order to obtain frequency spectrum of the analyzed signal. The FT based spectrum is no more used for the boundary detection and spectrum segmentation purpose. After this, the scale-space method has been applied in order to find the boundaries and segment the FBSE spectrum.

Then, EWT based filter bank (discussed in the previous section) has been generated and meaningful modes have been extracted. The NHT has been applied on each of the reconstructed sub-band signals in order to determine IA and IF functions and TF representation of the analyzed signal has been obtained. The block diagram of the proposed FBSE-EWT method has been depicted in Fig. 3. The SB stands for sub-band signals. Finally, proposed FBSE-EWT based TF representation has been compared with existing EWT and HHT based TF representations (discussed in the introduction section). It should be noted that EWT based TF representation has been obtained after applying NHT to the sub-band signals obtained using existing EWT method. For HHT based TF representation, we have applied NHT to the IMFs obtained through EMD method.

3.1. Performance evaluation

The performance of the TF representation has been quantitatively measured by computing mean square error (MSE) between the expected TF representation and the obtained TF representation of the considered multi-component synthetic signals (discussed latter). The expected TF representation is obtained by applying NHT to the prior known individual signal components of the considered multi-component synthetic signals. Finally, the MSE is expressed as,

$$\mathrm{MSE} = \frac{1}{PQ}\sum_{f=1}^{P}\sum_{t=1}^{Q}(\mathrm{TF}_1(f,t) - \mathrm{TF}(f,t))^2 \tag{26}$$

where, P and Q denote the total number of frequency points and total number of time instants in the TF plane, respectively. The TF_1 and TF denote the expected and obtained TF representations, respectively.

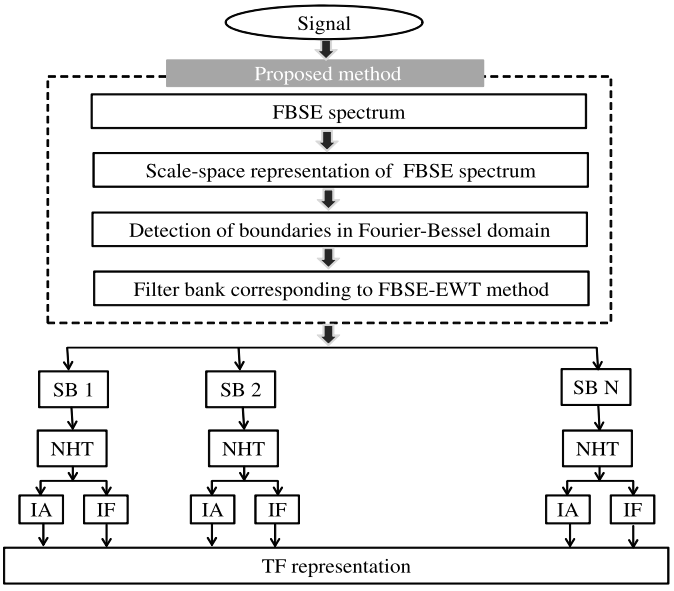

Fig. 3. Block diagram of the proposed FBSE-EWT based TF representation.

4. Experimental results

In the following sub-sections, we have considered multi-component AM and FM signals, as well as real EEG signals for the TF representation using proposed FBSE-EWT method. The performance of TF representation of the proposed method has also been compared with HHT and EWT methods.

4.1. TF representation of synthetic multi-component AM signals

We have considered synthetic multi-component AM signal expressed as, $y(t) = \sum_{i=1}^{3} 0.2(1 + 0.3\cos(2\pi t))\cos(2\pi f_i t)$ where three different cases have been considered, namely:

Case 1: $f_1 = 9$ Hz, $f_2 = 10$ Hz, $f_3 = 11$ Hz
Case 2: $f_1 = 9$ Hz, $f_2 = 11$ Hz, $f_3 = 13$ Hz
Case 3: $f_1 = 9$ Hz, $f_2 = 12$ Hz, $f_3 = 15$ Hz

In the first case, the signal components are very closely spaced in frequency-domain. The, frequency spacing among the components have been increased in cases 2 and 3. In all the cases, the signal duration is considered as 6 s with a sampling rate of 200 Hz. The multi-component AM signals for all the three cases have been shown in Fig. 4 and their expected TF representation is shown in Fig. 5. The intention behind the consideration of the above three cases is, whether the proposed FBSE-EWT method can reproduce each of the signal components in the TF plane without interference. For each of the cases, the performance of the proposed FBSE-EWT method has been compared with HHT and existing EWT method. The obtained TF representations of the three considered cases using HHT method have been shown in Fig. 6. It can be noticed that, in the first case, the signal components are hardly identifiable. In the second and third cases, three signal components are separable in the TF plane, but they are affected by interference. For EWT based TF representation, the boundary frequencies are not optimally detected in the FT spectrum when first two cases have been considered, as shown in Fig. 7 (first column). This resulted into formation of undesired EWT based filter-bank for these two cases (second column of Fig. 7). The EWT based TF representations for the three considered cases have been presented in Fig. 8. It can be observed that, EWT clearly reproduces three individual signal components in the TF plane for the third case

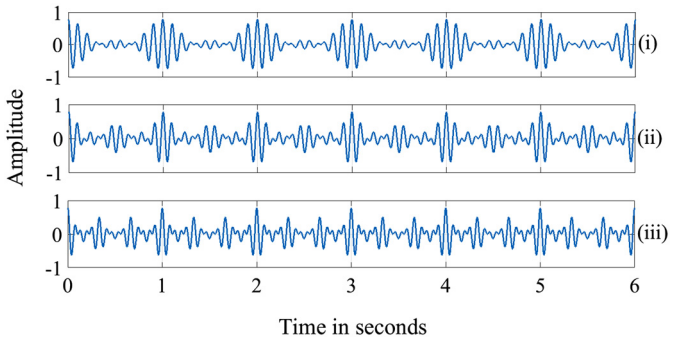

Fig. 4. Plots of the multi-component AM signals: (i) Case 1, (ii) Case 2, and (iii) Case 3.

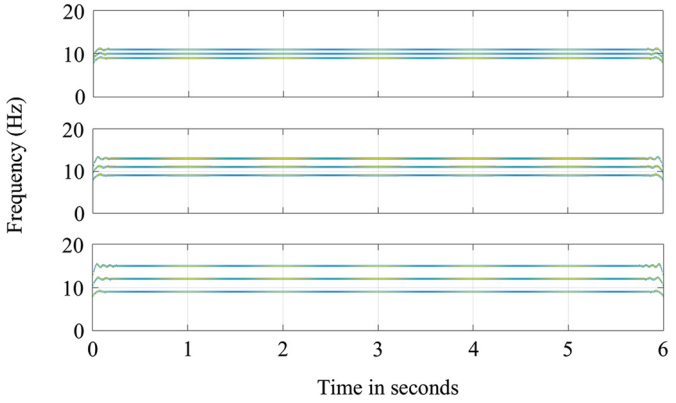

Fig. 5. Plots of the expected TF representation of multi-component AM signals for Case 1 (top), Case 2 (middle), and Case 3 (bottom).

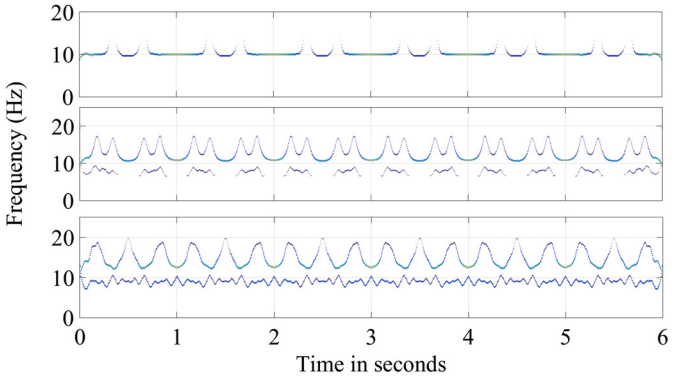

Fig. 6. Plots of the HHT based TF representation of multi-component AM signal for Case 1 (top), Case 2 (middle), and Case 3 (bottom).

only. Thus, EWT method is not able to represent closely spaced frequency components in the TF plane. For all the three cases, the detected boundaries in the FBSE domain and FBSE-EWT based filter banks have been presented in first and second column of Fig. 9, respectively. It can be seen in the figure that, for case 2, the boundary frequencies are optimally detected in the FBSE domain as compared to in FT domain (shown in Fig. 7). This is due to the fact that, FBSE spectrum provides better frequency resolution as compared to FT spectrum. The TF representation of all the three considered cases using proposed FBSE-EWT method has been presented in Fig. 10. It is clear from the figures that, except for the first case, proposed FBSE-EWT method clearly represents all the signal components in the TF plane. Thus, for case 1, none of the methods is able to represent the frequency components in the TF plane. Table 2 presents the MSE values for the HHT, EWT, and proposed FBSE-EWT method when above mentioned three cases of

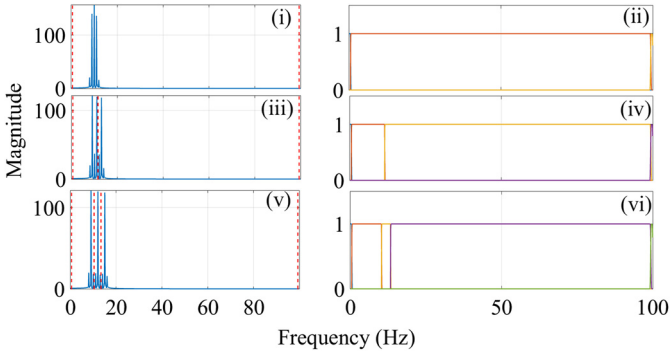

Fig. 7. Plots of (i) the detected boundaries in the FT spectrum and (ii) EWT based filter-bank for multi-component AM signal corresponding to Case 1. Plots of (iii) the detected boundaries in the FT spectrum and (iv) EWT based filter-bank for multi-component AM signal corresponding to Case 2. Plots of (v) the detected boundaries in the FT spectrum and (vi) EWT based filter-bank for multi-component AM signal corresponding to Case 3.

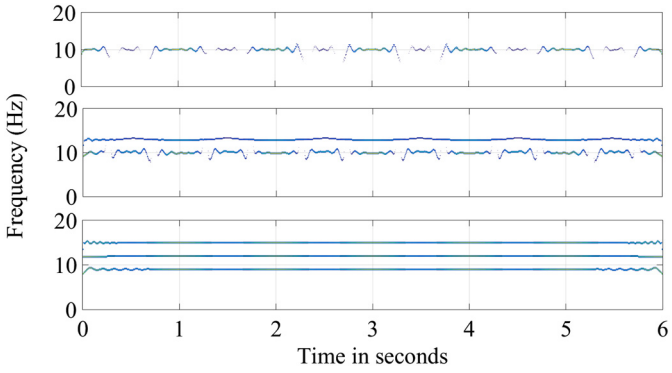

Fig. 8. Plots of EWT based TF representations of multi-component AM signals corresponding to case 1 (top), case 2 (middle), and case 3 (bottom).

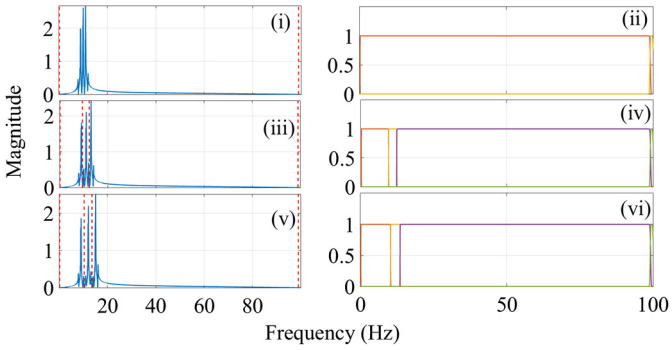

Fig. 9. Plots of (i) the detected boundaries in the FBSE spectrum, (ii) FBSE-EWT based filter-bank for multi-component AM signal corresponding to Case 1. Plots of (iii) the detected boundaries in the FBSE spectrum and (iv) FBSE-EWT based filter-bank for multi-component AM signal corresponding to Case 2. Plots of (v) the detected boundaries in the FBSE spectrum and (vi) FBSE-EWT based filter-bank for multi-component AM signal corresponding to Case 3.

the multi-component AM signals have been considered. For case 1, the MSE values are not considerable as none of the methods was successful in representing multi-component AM signal. For case 2, the MSE values for FBSE-EWT method is the lowest followed by EWT and HHT methods. Such kind of results were expected. For case 3, the MSE value for FBSE-EWT method is lower than EWT based method, whereas MSE for EMD method was the highest. This is because, the TF representation using EMD method has spurious or unwanted frequencies and interference terms which give rise to higher MSE value.

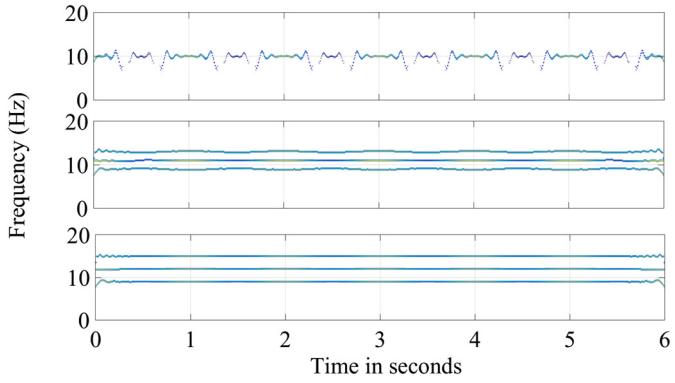

Fig. 10. Plots of FBSE-EWT based TF representation of multi-component AM signals corresponding to case 1 (top), case 2 (middle), and case 3 (bottom).

Table 2
Comparison of the MSE values of multi-component AM signal for different considered cases using FBSE-EWT, EWT, and HHT methods.

Cases	FBSE-EWT	EWT	HHT
Case 1	3.924×10^{-4}	3.973×10^{-4}	2.837×10^{-4}
Case 2	1.983×10^{-4}	3.794×10^{-4}	3.742×10^{-4}
Case 3	2.972×10^{-5}	3.66×10^{-5}	3.662×10^{-4}

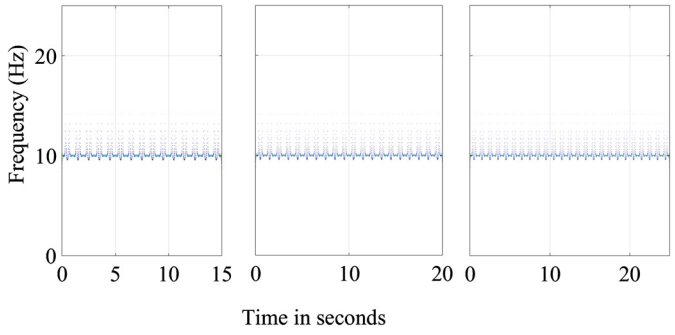

Fig. 11. Plots of the HHT based TF representation of multi-component AM signals for *subcase 1* (left most), *subcase 2* (middle), and *subcase 3* (right most).

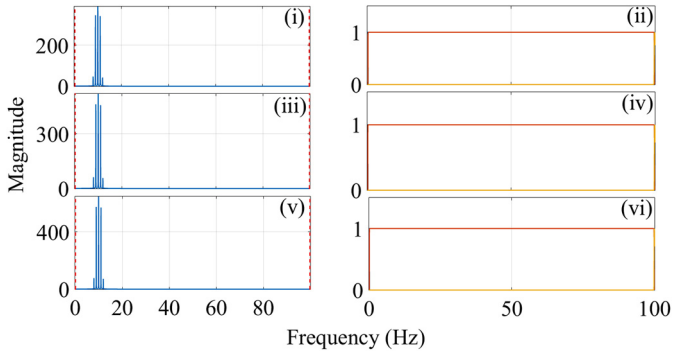

Fig. 12. Plots of (i) the detected boundaries in the FT spectrum and (ii) EWT based filter-bank of multi-component AM signal for *subcase 1*. Plots of the (iii) detected boundaries in the FT spectrum and (iv) EWT based filter-bank of multi-component AM signal for *subcase 2*. Plots of (v) the detected boundaries in the FT spectrum and (vi) EWT based filter-bank of multi-component AM signal for *subcase 3*.

In order to observe the effect of signal duration in the detection of optimal boundary frequencies, we have increased the signal duration of the case 1 multi-component AM signal and considered three different subcases as follows: *subcase 1*: signal duration of 15 s, *subcase 2*: signal duration of 20 s, and *subcase 3*: signal duration of 25 s. The TF representation using HHT method for three different subcases have been shown in Fig. 11. It can

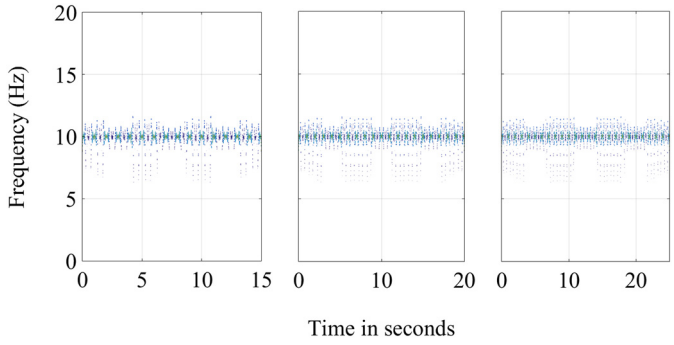

Fig. 13. Plots of EWT based TF representation of multi-component AM signals corresponding to *subcase 1* (left most), *subcase 2* (middle), and *subcase 3* (right most).

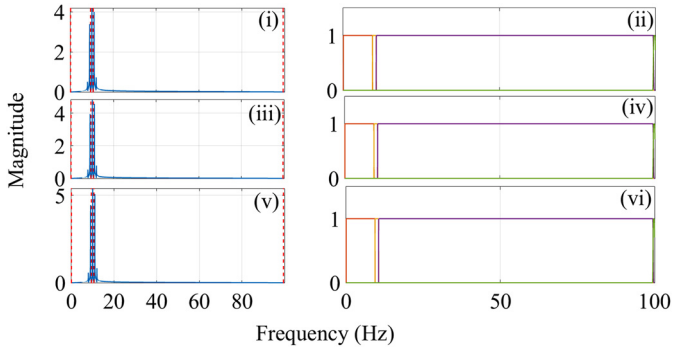

Fig. 14. Plots of the (i) detected boundaries in the FBSE spectrum and (ii) FBSE-EWT based filter-bank for multi-component AM signal corresponding to *subcase 1*. Plots of (iii) the detected boundaries in the FBSE spectrum and (iv) FBSE-EWT based filter-bank for multi-component AM signal corresponding to *subcase 2*. Plots of (v) the detected boundaries in the FBSE spectrum and (vi) FBSE-EWT based filter-bank for multi-component AM signal corresponding to *subcase 3*.

be observed that signal components overlap with each other in the TF plane. Thus, HHT method fails to represent closely spaced frequency components in the TF plane. For each of the considered subcases, the detected boundaries in the FT spectrum and EWT based filter banks have been shown in the first and second columns of Fig. 12. It is clear from the figure that boundaries are erroneously detected which resulted into formation of undesired EWT based filter bank. The TF representations using EWT method for the above mentioned subcases have been presented in Fig. 13. Hence, EWT method is not able to represent the closely spaced frequency components, even for increased signal durations. The detected boundary frequencies in the FBSE domain for all three subcases have been shown in the first column, where as the corresponding filter banks have been presented in the second column of Fig. 14. The figure shows that optimal boundary frequencies have been detected in the FBSE domain even for closely spaced frequency components. However, it can be noticed in Figs. 12 and 14 that, for all the considered subcases, though FT based spectrum also has three signal components like as FBSE spectrum, but the optimal boundary frequencies are detected in the FBSE spectrum only. The reason is explained with Fig. 15, which presents the plots of scale-space planes for the FT and FBSE spectrums corresponding to subcase 3. It is clear in the figure that in both the spectrums, six initial minima points are detected. This led to six scale-space curves (located at initial minima points) of different lengths in each of the scale-space plane. However, after length based thresholding operation, only first (located around zero frequency) and last (located around maximum frequency) scale-space curves are retained in the scale-space plane of FT spectrum. Thus, scale-space method detects only two boundary frequencies (corresponding to location of retained scale-space curves) and fails to

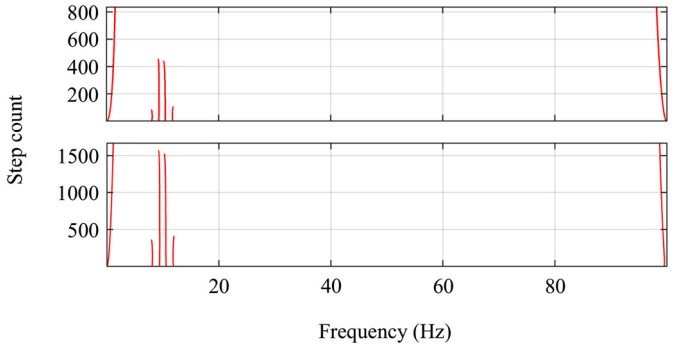

Fig. 15. Plots of scale-space planes for FT (top) and FBSE (bottom) spectrums corresponding to *subcase 3*.

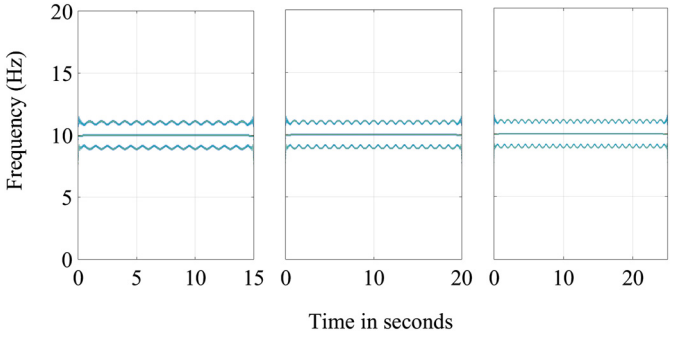

Fig. 16. Plots of FBSE-EWT based TF representation of multi-component AM signals corresponding to *subcase 1* (left most), *subcase 2* (middle), and *subcase 3* (right most).

detect other two desired boundary frequencies in the FT spectrum. This is in contrast to FBSE spectrum, where, four scale-space curves are chosen after thresholding. Thus, in FBSE spectrum four boundary frequencies are detected which include two desired boundary frequencies in between the closely spaced frequency components (9 Hz, 10 Hz, and 11 Hz). The TF representations for all the considered subcases using FBSE-EWT method are presented in Fig. 16 which clearly represent closely spaced frequency components in the TF plane. Thus, proposed FBSE-EWT provides better TF representation for the above considered subcases in comparison to HHT and existing EWT methods. Table 3 presents the MSE values for FBSE-EWT, EWT, and HHT based TF representations considering all the three subcases. As expected, the MSE values for FBSE-EWT based TF representation have been found lower in value as compared to HHT and EWT based TF representation for all the subcases.

4.2. TF representation of synthetic multi-component FM signals

In this subsection, we have considered a multi-component FM signal $y(t)$ expressed as,

$$y(t) = y_1(t) + y_2(t)$$

where $y_1(t)$ is a sinusoidally FM signal and $y_2(t)$ is a linearly FM chirp signal. These signals are mathematically expressed as

$$y_1(t) = \cos\left(2\pi\left(20t + 4\cos(0.54t)\right)\right)$$
$$y_2(t) = \cos\left(2\pi\left(f_4 t + 0.4t^2\right)\right)$$

where three distinct cases have been considered as,

Case 1: $f_4 = 9$ Hz.
Case 2: $f_4 = 10$ Hz.
Case 3: $f_4 = 11$ Hz.

Table 3
Comparison of the MSE values of multi-component AM signal for different considered subcases using FBSE-EWT, EWT, and HHT methods.

Subcases	FBSE-EWT	EWT	HHT
Subcase 1	1.126×10^{-4}	1.797×10^{-4}	1.327×10^{-4}
Subcase 2	9.399×10^{-5}	1.402×10^{-4}	1.012×10^{-4}
Subcase 3	7.29×10^{-5}	1.141×10^{-4}	8.204×10^{-5}

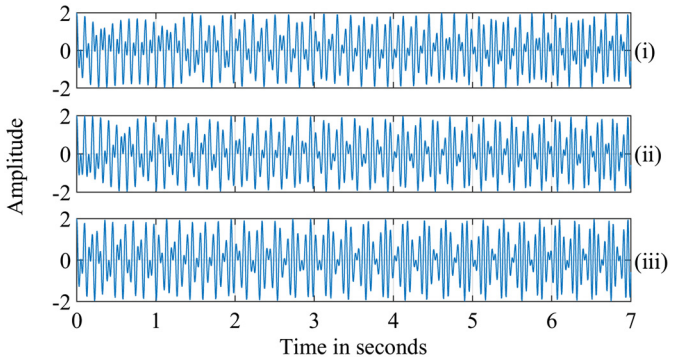

Fig. 17. Plots of the multi-component FM signals: (i) Case 1, (ii) Case 2, and (iii) Case 3.

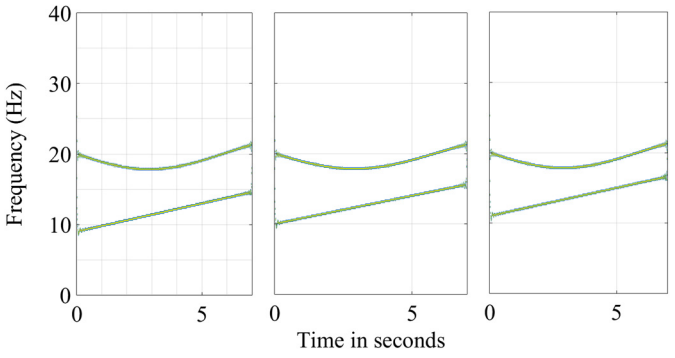

Fig. 18. Plots of the expected TF representation of multi-component FM signals corresponding to case 1 (left most), case 2 (middle), and case 3 (right most).

In case 1, the signal components $y_1(t)$ and $y_2(t)$ have comparatively higher frequency spacing as compared to Case 2 and Case 3. The frequency spacing between $y_1(t)$ and $y_2(t)$ is the lowest in Case 3 among the three cases. In all the cases, we have considered signal duration of 7 s with a sampling rate of 200 Hz. The synthetic multi-component FM signals corresponding to all the cases have been shown in Fig. 17 and their expected TF representations are depicted in Fig. 18. We have generated TF plane for all the three cases using the proposed FBSE-EWT method as well as with existing HHT and EWT methods. Fig. 19 presents the HHT based TF representation corresponding to three considered cases of multi-component FM signals. It can be observed from the figure that, HHT based TF representation suffers from interference terms. This is because of the mode mixing problem encountered by EMD method and the computation of correct IFs become difficult. Fig. 20 presents the detected boundaries in the FT spectrum (first column), and the generated filter banks (second column) corresponding to the three considered cases. The EWT based TF representation corresponding to above three cases of multi-component FM signals have been presented in Fig. 21. It can be noticed that EWT method has provided better TF representation as compared to HHT representation. However, the EWT based TF representation is not completely free from the presence of interference terms in the TF plane. The detected boundaries in the FBSE domain and the formed FBSE-EWT filter banks are shown in the first and second column of the Fig. 22, respectively. The TF representation based on

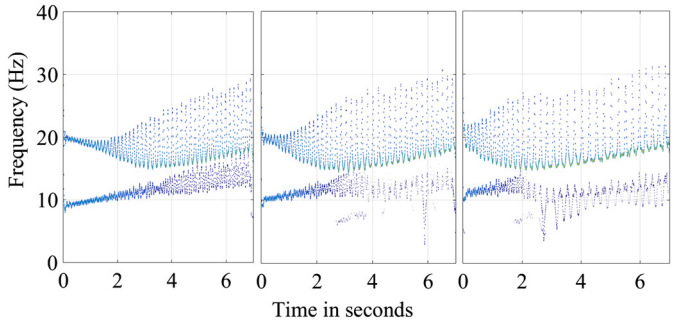

Fig. 19. Plots of HHT based TF representation of multi-component FM signals corresponding to case 1 (left most), case 2 (middle), and case 3 (right most).

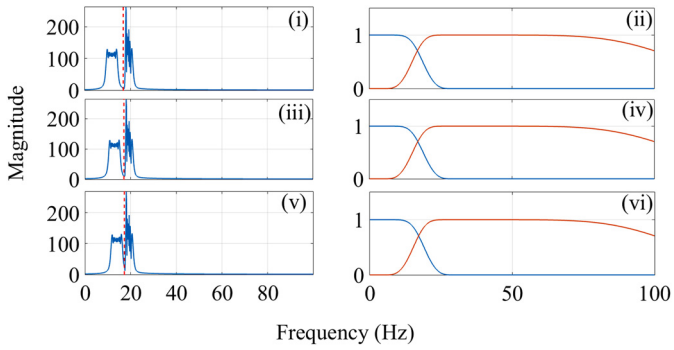

Fig. 20. Plots of (i) the detected boundaries in the FT spectrum and (ii) EWT based filter-bank for multi-component FM signal corresponding to Case 1. Plots of (iii) the detected boundaries in the FT spectrum and (iv) EWT based filter-bank for multi-component FM signal corresponding to Case 2. Plots of (v) the detected boundaries in the FT spectrum and (vi) EWT based filter-bank for multi-component FM signal corresponding to Case 3.

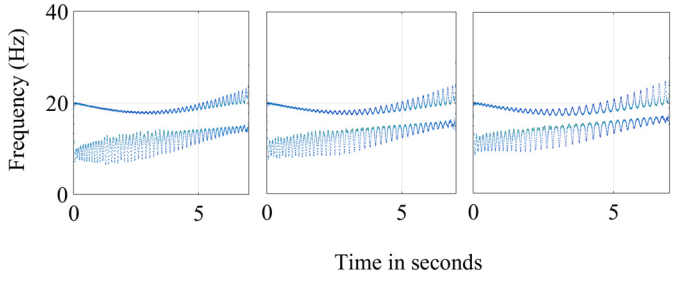

Fig. 21. Plots of EWT based TF representation of multi-component FM signals corresponding to case 1 (left most), case 2 (middle), and case 3 (right most).

FBSE-EWT method corresponding to three considered cases have been presented in Fig. 23. It can be observed from the figure that, FBSE-EWT method clearly represents the multi-component FM signals in the TF plane. Table 4 presents the MSE values of all the studied TF representation methods for all the considered cases. It can be observed that, the MSE values for the proposed FBSE-EWT method are less in comparison to HHT, and EWT methods. These results are corresponding to the obtained TF representations using FBSE-EWT, EWT, and HHT methods.

4.3. TF representation of real electroencephalogram signals

We have applied the proposed FBSE-EWT method for the TF representation of real epileptic seizure EEG signal. The EEG signal used in this paper is made available publicly by University of Bonn, Germany [50]. The EEG signal has a sampling rate of 173.61 Hz with a duration of 23.6 s. In this work, we have obtained the TF representation of the 8 s duration segment of the EEG signal, as shown in Fig. 24. The TF representation using FBSE-EWT method

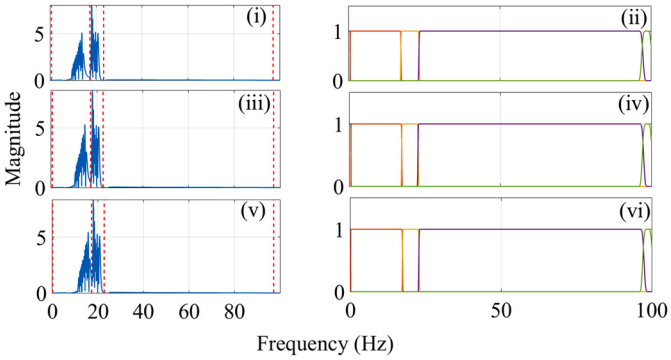

Fig. 22. Plots of (i) the detected boundaries in the FBSE spectrum, (ii) FBSE-EWT based filter-bank for multi-component FM signal corresponding to Case 1. Plots of (iii) the detected boundaries in the FBSE spectrum and (iv) FBSE-EWT based filter-bank for multi-component FM signal corresponding to Case 2. Plots of (v) the detected boundaries in the FBSE spectrum and (vi) FBSE-EWT based filter-bank for multi-component FM signal corresponding to Case 3.

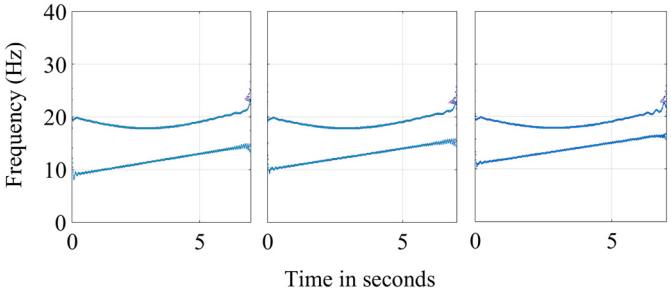

Fig. 23. Plots of FBSE-EWT based TF representation of multi-component FM signals corresponding to case 1 (left most), case 2 (middle), and case 3 (right most).

Table 4
Comparison of the MSE values of multi-component FM signal for different considered cases using FBSE-EWT, EWT, and HHT methods.

Cases	FBSE-EWT	EWT	HHT
Case 1	0.0015	0.0043	0.0048
Case 2	0.0015	0.0044	0.0051
Case 3	0.0015	0.0045	0.0053

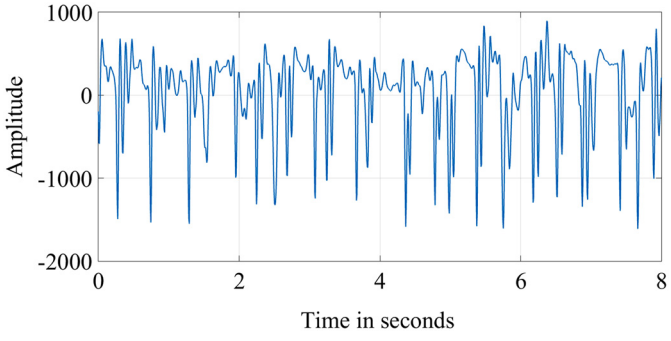

Fig. 24. Plot of real EEG signal.

has been compared with HHT and existing EWT method. It can be seen from the Fig. 25 that, HHT based TF representation generates spurious frequencies in TF plane and suffers from interference. The EWT based TF representation has been shown in Fig. 26(iii), where as the detected boundaries in the FT spectrum and EWT based filter banks for the real EEG signal have been shown in Fig. 26(i) and (ii), respectively. It is clear from the figure that EWT method generates unwanted and mostly scattered IFs. This is because, some of the EWT generated sub-band signals are wide-band frequency components due to improper detection of boundary fre-

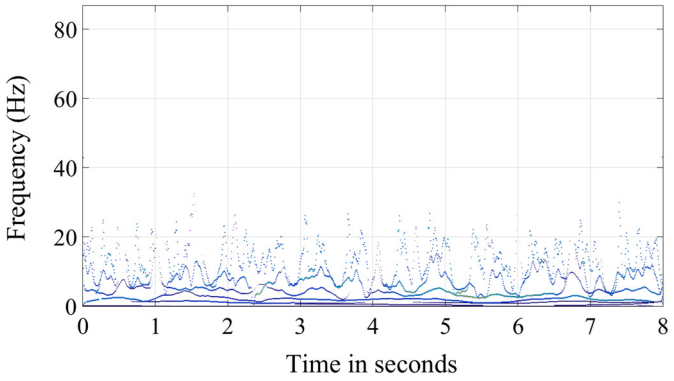

Fig. 25. Plot of HHT based TF representation of real EEG signal.

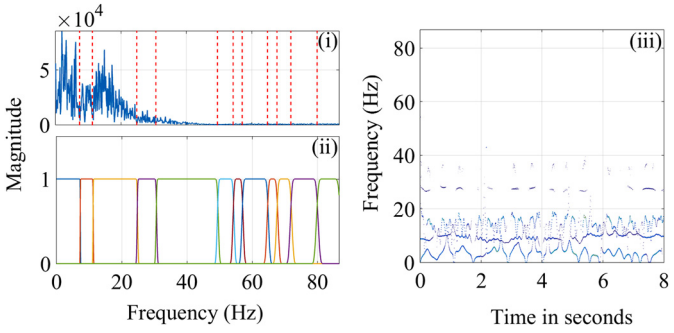

Fig. 26. Plots of (i) the detected boundaries in the FT spectrum, (ii) generated EWT based filter bank, and (iii) EWT based TF representation of real EEG signal.

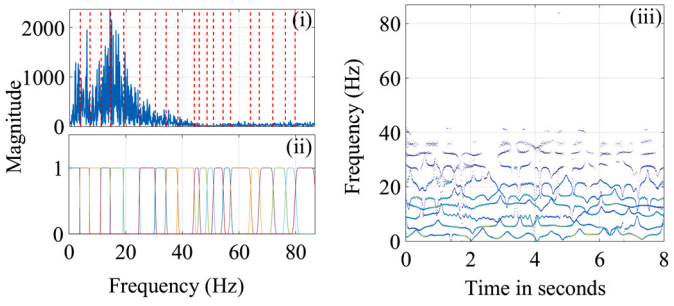

Fig. 27. Plots of (i) the detected boundaries in the FBSE spectrum, (ii) generated FBSE-EWT based filter bank, and (iii) FBSE-EWT based TF representation of real EEG signal.

quencies in the FT spectrum. The detected boundaries in the FBSE domain, the FBSE-EWT based filter bank, and obtained FBSE-EWT based TF representation have been shown in Fig. 27(i), (ii), and (iii), respectively. It should be noted that almost all the sub-band signals generated using FBSE-EWT method are narrow-band in nature. This helps to compute the more meaningful IF using NHT. In HHT and EWT based TF representations, it is difficult to interpret the frequency components above 15 Hz as they are mostly scattered and not well connected. However, the FBSE-EWT provides more clear TF representation of the frequency components in low as well as in high frequency regions. Thus, FBSE-EWT has clear advantage over EWT and HHT in the TF representation of non-stationary signals.

5. Discussion

In the previous section, we have presented the performance of the proposed FBSE-EWT based TF representation method and compared with HHT and existing EWT methods. The obtained results demonstrate that proposed FBSE-EWT provides better TF representation as compared to HHT and EWT methods especially when analyzed signals have closely spaced frequency component. The existing EWT method is not successful to estimate the desired boundary frequencies when signal frequency components are very closely spaced. This is due to low frequency resolution of FT spectrum. It also becomes very difficult to identify components in FT spectrum when the analyzed signal is of short duration. On the other hand, FBSE spectrum has twice frequency resolution as compared to FT spectrum. Thus, it is more advantageous to use FBSE spectrum as compared to FT spectrum in order to estimate the optimal boundary frequencies. There exist several algorithms for the efficient computation of FBSE coefficients such as: expansion of the function into Gaussian–Laguerre (G-L) functions [51], using interpolated FFT values of the function given [42], dual algorithm based on Fourier selection summation method and Bessel function large argument asymptotic expansion [52], one-dimensional FT followed by iterated additions of preselected Fourier components [53]. These algorithms can be used for computation of FB coefficients in faster way. In the literature, there has been effort for estimating the optimal boundary frequencies in order to build wavelet based filter bank. In [32], authors replaced FT spectrum with multiple signal classification (MUSIC) spectrum for estimating the optimal boundary frequencies. However, the model order is required in advance for the MUSIC spectrum. In Fig. 28, we have presented the MUSIC-EWT based TF representation for multi-component AM signal of case 3 (discussed in subsection 4.1) with model orders 4 and 6, respectively. The respective boundary frequencies and MUSIC-EWT based filter banks are also shown in the figure. It can be seen that MUSIC-EWT provides desired TF representation for order 6. The problem can be more severe in case of the TF representation of non-stationary signals like EEG signals where prior information of number of signal components are unknown. In Figs. 29 and 30, we have presented the MUSIC-EWT based TF representation of real EEG signal (discussed in section 4.3) for model orders 6 and 20, respectively. It can be seen that, MUSIC-EWT achieved better TF representation with model order 20. Thus, if the number of components in the signal is unknown, then a fine tuning is recommended in the MUSIC-EWT algorithm. However, our method does not require any prior information about the presence of number of signal components. The method presented in this paper is suitable for the TF representation of the signals whose components do not overlap in frequency-domain. If the signal components overlap in frequency-domain, obtaining optimal boundary frequencies for segmenting the spectrum will be difficult. In future, it will be interesting to develop EWT based algorithm for representing signals whose components overlap in frequency domain but disjoint in TF plane.

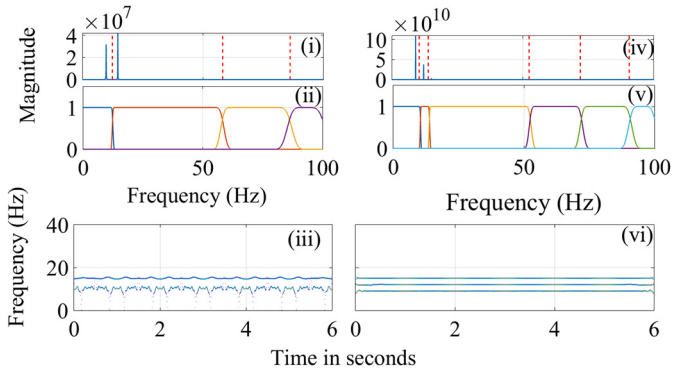

Fig. 28. Plot of (i) the detected boundaries in the MUSIC spectrum (model order = 4), (ii) MUSIC-EWT based filter-bank, and (iii) MUSIC-EWT based TF representation for multi-component AM signal of case 3. Plot of (iv) the detected boundaries in the MUSIC spectrum (model order = 6), (v) MUSIC-EWT based filter-bank, and (vi) MUSIC-EWT based TF representation for multi-component AM signal of case 3.

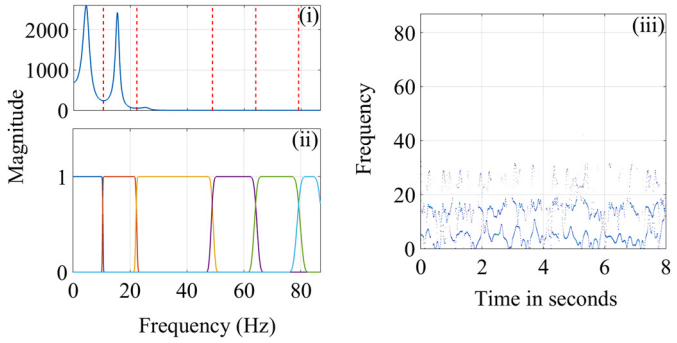

Fig. 29. Plots of (i) the detected boundaries in the MUSIC spectrum (model order = 6), (ii) MUSIC-EWT based filter-bank, and (iii) MUSIC-EWT based TF representation of real EEG signal.

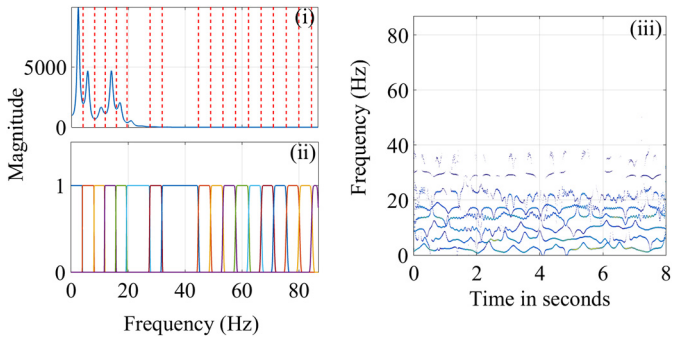

Fig. 30. Plots of (iv) the detected boundaries in the MUSIC spectrum (model order = 20), (v) MUSIC-EWT based filter-bank, and (vi) MUSIC-EWT based TF representation of real EEG signal.

6. Conclusion

We have presented a new FBSE-EWT method for the TF representation of non-stationary signals. The FT spectrum has been replaced with FBSE spectrum for the estimation of optimal boundary frequencies, which resulted into improved wavelet based filter bank. The proposed method has been applied to multi-component AM signals, multi-component FM signals, and real EEG signals for TF representation. The TF representation performances also have been quantitatively evaluated using MSE measure. The experimental results indicate that the proposed algorithm provides better TF representation in comparison to existing EWT method and HHT method. Thus, the proposed FBSE-EWT method has potential to analyse wide classes of real life non-stationary signals.

References

[1] B. Boashash, Time–Frequency Signal Analysis and Processing: A Comprehensive Reference, Academic Press, Oxford, UK, 2003.
[2] A. Bhattacharyya, R.B. Pachori, A. Upadhyay, U.R. Acharya, Tunable-Q wavelet transform based multiscale entropy measure for automated classification of epileptic EEG signals, Appl. Sci. 7 (4) (2017) 385.
[3] R.B. Pachori, Discrimination between ictal and seizure-free EEG signals using empirical mode decomposition, Res. Lett. Signal Process. (2008) 2008, p. 14.
[4] A. Bhattacharyya, R.B. Pachori, U.R. Acharya, Tunable-Q wavelet transform based multivariate sub-band fuzzy entropy with application to focal EEG signal analysis, Entropy 19 (3) (2017) 99.
[5] S. Patidar, R.B. Pachori, Classification of cardiac sound signals using constrained tunable-Q wavelet transform, Expert Syst. Appl. 41 (16) (2014) 7161–7170.
[6] S. Lahmiri, A variational mode decomposition approach for analysis and forecasting of economic and financial time series, Expert Syst. Appl. 55 (2016) 268–273.
[7] F. Amini, N.K. Hazaveh, A.A. Rad, Wavelet PSO-based LQR algorithm for optimal structural control using active tuned mass dampers, Comput.-Aided Civ. Infrastruct. Eng. 28 (7) (2013) 542–557.
[8] M. O'Byrne, F. Schoefs, B. Ghosh, V. Pakrashi, Texture analysis based damage detection of ageing infrastructural elements, Comput.-Aided Civ. Infrastruct. Eng. 28 (3) (2013) 162–177.
[9] M. Portnoff, Time–frequency representation of digital signals and systems based on short-time Fourier analysis, IEEE Trans. Acoust. Speech Signal Process. 28 (1) (1980) 55–69.
[10] I. Daubechies, Ten Lectures on Wavelets, CBMS–NSF Reg. Conf. Ser. Appl. Math., vol. 61, SIAM, Philadelphia, PA, USA, 1992.
[11] N.E. Huang, Z. Shen, S.R. Long, M.C. Wu, H.H. Shih, Q. Zheng, N.-C. Yen, C.C. Tung, H.H. Liu, The empirical mode decomposition and the Hilbert spectrum for nonlinear and non-stationary time series analysis, Proc. R. Soc. Lond. A, Math. Phys. Eng. Sci. 454 (1998) 903–995.
[12] E. Sejdić, I. Djurović, J. Jiang, Time–frequency feature representation using energy concentration: an overview of recent advances, Digit. Signal Process. 19 (1) (2009) 153–183.
[13] M. Valtierra-Rodriguez, R. de Jesus Romero-Troncoso, R.A. Osornio-Rios, A. Garcia-Perez, Detection and classification of single and combined power quality disturbances using neural networks, IEEE Trans. Ind. Electron. 61 (5) (2014) 2473–2482.
[14] H. Tao, J.M. Zain, M.M. Ahmed, A.N. Abdalla, W. Jing, A wavelet-based particle swarm optimization algorithm for digital image watermarking, Integr. Comput.-Aided Eng. 19 (1) (2012) 81–91.
[15] G. Pérez, A. Conci, A.B. Moreno, J.A. Hernandez-Tamames, Rician noise attenuation in the wavelet packet transformed domain for brain MRI, Integr. Comput.-Aided Eng. 21 (2) (2014) 163–175.
[16] X. Jiang, H. Adeli, Wavelet packet-autocorrelation function method for traffic flow pattern analysis, Comput.-Aided Civ. Infrastruct. Eng. 19 (5) (2004) 324–337.
[17] I.W. Selesnick, Wavelet transform with tunable Q-factor, IEEE Trans. Signal Process. 59 (8) (2011) 3560–3575.
[18] I. Daubechies, J. Lu, H.-T. Wu, Synchrosqueezed wavelet transforms: an empirical mode decomposition-like tool, Appl. Comput. Harmon. Anal. 30 (2) (2011) 243–261.
[19] K. Dragomiretskiy, D. Zosso, Variational mode decomposition, IEEE Trans. Signal Process. 62 (3) (2014) 531–544.
[20] A. Upadhyay, R.B. Pachori, Instantaneous voiced/non-voiced detection in speech signals based on variational mode decomposition, J. Franklin Inst. 352 (7) (2015) 2679–2707.
[21] A. Upadhyay, R.B. Pachori, Speech enhancement based on mEMD–VMD method, Electron. Lett. 53 (7) (2017) 502–504.
[22] N.E. Huang, Z. Wu, S.R. Long, K.C. Arnold, X. Chen, K. Blank, On instantaneous frequency, Adv. Adapt. Data Anal. 1 (02) (2009) 177–229.
[23] Z. Yang, L. Yang, C. Qing, D. Huang, A method to eliminate riding waves appearing in the empirical AM/FM demodulation, Digit. Signal Process. 18 (4) (2008) 488–504.
[24] Z. Wu, N.E. Huang, Ensemble empirical mode decomposition: a noise-assisted data analysis method, Adv. Adapt. Data Anal. 1 (01) (2009) 1–41.
[25] P. Singh, S.D. Joshi, R.K. Patney, K. Saha, The Fourier decomposition method for nonlinear and non-stationary time series analysis, Proc. R. Soc. A 473 (2017) 20160871.
[26] G.K. Apostolidis, L.J. Hadjileontiadis, Swarm decomposition: a novel signal analysis using swarm intelligence, Signal Process. 132 (2017) 40–50.
[27] R.R. Sharma, R.B. Pachori, Time–frequency representation using IEVDHM-HT with application to classification of epileptic EEG signals, IET Sci. Meas. Technol. 12 (1) (2017) 72–82.
[28] R.B. Pachori, P. Sircar, A new technique to reduce cross terms in the Wigner distribution, Digit. Signal Process. 17 (2) (2007) 466–474.
[29] R.B. Pachori, A. Nishad, Cross-terms reduction in the Wigner–Ville distribution using tunable-Q wavelet transform, Signal Process. 120 (2016) 288–304.
[30] J. Gilles, Empirical wavelet transform, IEEE Trans. Signal Process. 61 (16) (2013) 3999–4010.
[31] A. Bhattacharyya, R.B. Pachori, A multivariate approach for patient-specific EEG seizure detection using empirical wavelet transform, IEEE Trans. Biomed. Eng. 64 (9) (2017) 2003–2015.
[32] J.P. Amezquita-Sanchez, H. Adeli, A new music-empirical wavelet transform methodology for time–frequency analysis of noisy nonlinear and non-stationary signals, Digit. Signal Process. 45 (2015) 55–68.
[33] K. Gopalan, T.R. Anderson, E.J. Cupples, A comparison of speaker identification results using features based on cepstrum and Fourier–Bessel expansion, IEEE Trans. Speech Audio Process. 7 (3) (1999) 289–294.
[34] R.B. Pachori, P. Sircar, Analysis of multicomponent AM–FM signals using FB-DESA method, Digit. Signal Process. 20 (1) (2010) 42–62.
[35] P. Jain, R.B. Pachori, Time-order representation based method for epoch detection from speech signals, J. Intell. Syst. 21 (1) (2012) 79–95.
[36] J. Gilles, K. Heal, A parameterless scale-space approach to find meaningful modes in histograms—application to image and spectrum segmentation, Int. J. Wavelets Multiresolut. Inf. Process. 12 (06) (2014) 1450044.
[37] N. Otsu, A threshold selection method from gray-level histograms, IEEE Trans. Syst. Man Cybern. 9 (1) (1979) 62–66.
[38] J. Schroeder, Signal processing via Fourier–Bessel series expansion, Digit. Signal Process. 3 (2) (1993) 112–124.

[39] R.B. Pachori, P. Sircar, EEG signal analysis using FB expansion and second-order linear TVAR process, Signal Process. 88 (2) (2008) 415–420.
[40] P. Jain, R.B. Pachori, Event-based method for instantaneous fundamental frequency estimation from voiced speech based on eigenvalue decomposition of the Hankel matrix, IEEE/ACM Trans. Audio Speech Lang. Process. 22 (10) (2014) 1467–1482.
[41] R.B. Pachori, P. Sircar, Non-Stationary Signal Analysis: Methods Based on Fourier–Bessel Representation, LAP LAMBERT Academic Publishing, 2010.
[42] K. Gopalan, C. Chen, Numerical evaluation of Fourier–Bessel series expansion, in: IEEE International Conference on Acoustics, Speech, and Signal Processing, Vol. 8, ICASSP'83, 1983, pp. 151–154.
[43] L. Cohen, C. Lee, Instantaneous frequency, its standard deviation and multicomponent signals, Proc. SPIE, vol. 975, 1988, pp. 186–208.
[44] P. Maragos, J.F. Kaiser, T.F. Quatieri, Energy separation in signal modulations with application to speech analysis, IEEE Trans. Signal Process. 41 (10) (1993) 3024–3051.
[45] P. Jain, R.B. Pachori, An iterative approach for decomposition of multi-component non-stationary signals based on eigenvalue decomposition of the Hankel matrix, J. Franklin Inst. 352 (10) (2015) 4017–4044.
[46] J.L. Semmlow, B. Griffel, Biosignal and Medical Image Processing, CRC Press, 2014.
[47] R.B. Pachori, D. Hewson, Assessment of the effects of sensory perturbations using Fourier–Bessel expansion method for postural stability analysis, J. Intell. Syst. 20 (2) (2011) 167–186.
[48] A.S. Hood, R.B. Pachori, V.K. Reddy, P. Sircar, Parametric representation of speech employing multi-component AFM signal model, Int. J. Speech Technol. 18 (3) (2015) 287–303.
[49] A. Nuttall, E. Bedrosian, On the quadrature approximation to the Hilbert transform of modulated signals, Proc. IEEE 54 (10) (1966) 1458–1459.
[50] R.G. Andrzejak, K. Lehnertz, F. Mormann, C. Rieke, P. David, C.E. Elger, Indications of nonlinear deterministic and finite-dimensional structures in time series of brain electrical activity: dependence on recording region and brain state, Phys. Rev. E 64 (6) (2001) 061907.
[51] E. Cavanagh, B. Cook, Numerical evaluation of Hankel transforms via Gaussian–Laguerre polynomial expansions, IEEE Trans. Acoust. Speech Signal Process. 27 (4) (1979) 361–366.
[52] S. Candel, Dual algorithms for fast calculation of the Fourier–Bessel transform, IEEE Trans. Acoust. Speech Signal Process. 29 (5) (1981) 963–972.
[53] S. Candel, An algorithm for the Fourier–Bessel transform, Comput. Phys. Commun. 23 (4) (1981) 343–353.

Abhijit Bhattacharyya received the B.E. (Hons.) degree from the University of Burdwan, Bardhaman, India, and the M.Tech. degree from National Institute of Technology Jalandhar, Jalandhar, India, both in Electronics and Communication engineering, in 2010 and 2013, respectively. He is working towards Ph.D. degree in Discipline of Electrical Engineering at Indian Institute of Technology Indore, Indore, India. He was selected as a Raman-Charpak fellow in the year 2017. Currently in his Ph.D. duration, under Raman-Charpak fellowship he is working at the Research Centre for Automatics, Nancy, France/CRAN UMR 7039 University of Lorraine-CNRS. He has published seven papers in international journals and conferences. He has reviewed papers in IEEE Journal of Biomedical and Health Informatics, Multidimensional Systems and Signal Processing, Computers and Electrical Engineering journals. He is a student member of IEEE. His research interests include biomedical signal processing (with an emphasis to EEG signals), non-stationary signal processing, spatial filtering, and source separation.

Lokesh Singh graduated from Indian Institute of Technology (ISM) Dhanbad, India in 2013 with B.Tech. in Electronics and Communication Engineering. He served as a Mathematics faculty for IIT-JEE at Whizdome Educare, New Delhi, India during 2013–2014. Currently, he is working towards M.Tech. degree in Communication and Signal Processing from Discipline of Electrical Engineering at Indian Institute of Technology Indore, Indore, India. He is a student member of IEEE. His research interests include artificial intelligence and non-stationary signal processing.

Ram Bilas Pachori received the B.E. degree with honours in Electronics and Communication Engineering from Rajiv Gandhi Proudyogiki Vishwavidyalaya, Bhopal, India in 2001, the M.Tech. and Ph.D. degrees in Electrical Engineering from Indian Institute of Technology (IIT) Kanpur, Kanpur, India in 2003 and 2008 respectively. He worked as a Postdoctoral Fellow at Charles Delaunay Institute, University of Technology of Troyes, Troyes, France during 2007–2008. He served as an Assistant Professor at Communication Research Center, International Institute of Information Technology, Hyderabad, India during 2008–2009. He served as an Assistant Professor at Discipline of Electrical Engineering, IIT Indore, Indore, India during 2009–2013. He worked as an Associate Professor at Discipline of Electrical Engineering, IIT Indore, Indore, India during 2013–2017 where presently he has been working as a Professor since 2017. He worked as a Visiting Scholar at Intelligent Systems Research Center, Ulster University, Northern Ireland, UK during December 2014. He is an Associate Editor of Biomedical Signal Processing and Control journal and an Editor of IETE Technical Review journal. He is a senior member of IEEE and a Fellow of IETE. He has more than 125 publications which include journal papers, conference papers, book, and book chapters. His research interests are in the areas of biomedical signal processing, non-stationary signal processing, speech signal processing, signal processing for communications, computer-aided medical diagnosis, and signal processing for mechanical systems.